Fusion Engineering and Design 89 (2014) 1370–1374

Contents lists available at ScienceDirect

Fusion Engineering and Design

journal homepage: www.elsevier.com/locate/fusengdes

3D numerical study of pressure equalization in MHD flow in a rectangular duct with insulating flow channel insert

Damien Sutevski*, Sergey Smolentsev, Mohamed Abdou

UCLA Fusion Science and Technology Center, Los Angeles, CA, United States

HIGHLIGHTS

- We model MHD flow with a flow channel insert (FCI) and associated pressure equalization effects.
- Two pressure equalization (PE) mechanisms have been identified and studied.
- PE via electric currents appears to dominate compared to purely hydrodynamic PE.
- In our study, a PES does not contribute significantly to PE.

ARTICLE INFO

Article history:
Received 2 October 2013
Received in revised form 24 January 2014
Accepted 28 January 2014
Available online 6 April 2014

Keywords:
Flow channel insert
Pressure equalization
MHD
Liquid metal
Fringing field

ABSTRACT

A flow channel insert (FCI) made of a Silicon Carbide (SiC) composite or foam is the key element of the dual-coolant lead-lithium (DCLL) blanket concept. Pressure equalization openings in the FCI wall are designed to equalize possible pressure differences in the flowing liquid metal (LM) between the bulk flow inside the FCI box and that in the thin gap between the FCI and the outer ferritic steel duct, thus reducing the mechanical stress in the FCI. In the present study, the MHD flow and associated pressure equalization effects are simulated with a numerical code in 3D. Two pressure equalization mechanisms have been identified and studied: one is due to LM flow through the flow equalization slot, and the other is due to induced electric currents flowing across the non-ideally insulating FCI wall. The second effect appears to both dominate and provide a more effective way of pressure equalization compared to the purely hydrodynamic mechanism. Parametric studies have been performed to address the impact of the FCI electrical conductivity, slot size, and the duct length. Finally, recommendations on the FCI design are proposed to result in more effective pressure equalization.

1. Introduction

The idea of using SiC flow channel inserts (FCIs) for electrical and thermal insulation in ducts of a liquid metal (LM) blanket was first proposed by Malang et al. [1] and then intensively studied worldwide mostly as applied to the dual-coolant lead-lithium (DCLL) blanket concept, e.g. see [2].

In our previous 3D numerical study [3], pressure drop reduction by a SiC FCI was analyzed and compared with 2D numerical results [4] and experiments [5]. The pressure drop in the 3D numerical computations matched well with the experimental results but varied from the 2D numerical computations. This discrepancy led us to explore 3D effects. In this study we continue our numerical studies using HIMAG, a 3D, unstructured mesh, MHD solver [6]. We pay attention in particular to 3D effects to address the effectiveness of pressure equalization (PE) between the bulk flow and the gap flow on both sides of the FCI

In the original FCI concept, the PE is considered an important property of the FCI design since a high pressure difference in the liquid on both sides of the insert may lead to intolerably high mechanical stresses in the FCI. For consistency with previous studies, we use the same duct geometry and dimensions, including the outer conducting duct and the inner FCI box with and without a slot in one of the FCI walls, which are parallel to the magnetic field, for pressure equalization (Fig. 1). The internal FCI dimensions are $2a = 54$ mm (in the direction perpendicular to the magnetic field) and $2b = 46$ mm (in the direction parallel to the magnetic field). The thickness of the FCI wall is 2 mm. The default duct length L is 1.5 m, and the applied transverse magnetic field B_0 varies from 0.5 to 2.0 T, which corresponds to dimensionless Hartmann numbers 630–2500. The Hartmann number is defined by:

$$Ha = B_0 b \sqrt{\frac{\sigma}{\nu\rho}}, \quad (1)$$

* Corresponding author. Tel.: +1 3105742557.
E-mail address: damien@fusion.ucla.edu (D. Sutevski).

0920-3796/$ – see front matter © 2014 Elsevier B.V. All rights reserved.
http://dx.doi.org/10.1016/j.fusengdes.2014.01.076

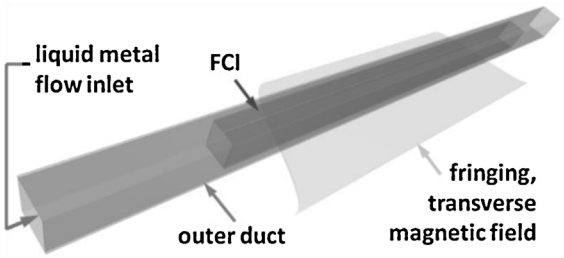

Fig. 1. This is the general configuration for the simulations in this study. The fringing magnetic field is entirely contained within the FCI.

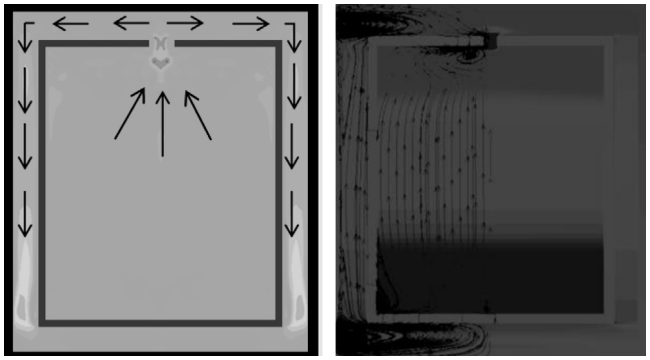

Fig. 2. The z-components of velocity show that the fluid moves through the slot to equalize the pressure (left). Contours show axial currents are present, and electric current lines show that, while the bulk is well insulated, there is leakage through the slot (right).

where σ is the electrical conductivity of the LM, and ρ and ν are kinematic viscosity and fluid density.

In accordance with the theoretical considerations of the PE mechanism suggested in [2], two pressure equalization methods are explored in this study: those associated with electromagnetic (Lorentz) forces with a conducting FCI (Fig. 2) and those with hydrodynamic forces with a slotted FCI (Fig. 3). Consider the Poisson equation for pressure, derived from taking the derivative of each projection of the momentum equation:

$$\frac{\partial^2 P}{\partial x^2} + \frac{\partial^2 P}{\partial y^2} + \frac{\partial^2 P}{\partial z^2} = S_P^V + S_P^J \tag{2}$$

where P is the pressure and S_P^V and S_P^J are source terms for fluid motion and pressure change due to electric current flows,

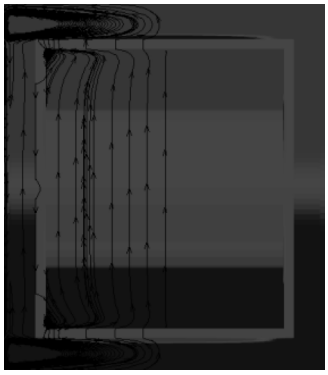

Fig. 3. Electric currents pass through the conducting FCI contributing toward pressure equalization between the bulk and gap flows.

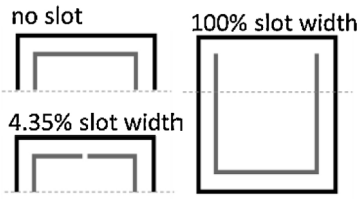

Fig. 4. These slot widths are visual examples of 0, 1, and 26 mm slot variations.

respectively.

$$S_p^v = \rho\frac{\partial}{\partial x}\left[\nu\nabla^2 U - U\frac{\partial U}{\partial x} - V\frac{\partial U}{\partial y} - W\frac{\partial U}{\partial z}\right] + \rho\frac{\partial}{\partial y}\left[\nu\nabla^2 V - U\frac{\partial V}{\partial x} - V\frac{\partial V}{\partial y} - W\frac{\partial V}{\partial z}\right] + \rho\frac{\partial}{\partial z}\left[\nu\nabla^2 W - U\frac{\partial W}{\partial x} - W\frac{\partial W}{\partial y} - W\frac{\partial W}{\partial z}\right] \tag{3}$$

$$S_p^J = \frac{\partial}{\partial x}\left(j_z B_y^0 - j_y B_z^0 + \frac{\partial}{\partial y}(j_x B_z^0 - j_z B^0 x)\right) + \frac{\partial}{\partial z}(j_y B_x^0 - j_x B_y^0) \tag{4}$$

These source terms (Eqs. (3) and (4)) separately capture the two mechanisms, and our goal is to indirectly assess their contributions.

The first mechanism assumes an axial pressure equalization slot (PES) in the FCI wall parallel to the magnetic field, which may be suitable for equalizing the pressure by allowing LM to flow between the bulk and gap regions. In this analysis, the FCI is ideally insulating to eliminate any effects on the pressure equalization associated with the electric currents that may cross the FCI. Electric currents are well insulated and retained in the bulk flow, though some leakage through the slot is present. Several computations were performed for varying slot widths to quantify its role in PE. We show that although a PES can help equalize the pressure difference, its effectiveness declines asymptotically over a small range of slot widths.

The second mechanism for PE is through Lorentz forces which allow some of the induced electric currents to pass through the FCI as discussed in [2]. In the set of computations where this mechanism is addressed, there is no slot, but the electrical conductivity of the FCI is varied from zero to values comparable with the electrical conductivity of the LM. Physically, the associated time scale would be very small, relative to the prior mechanism, and PE effects rapid. This mechanism is more effective in equalizing the pressure between the bulk and gap flows, but in practice, the FCI insulating requirements and physical properties of SiC limit the range of allowable electrical conductivities to $\sim 10^2$ S/m [7]. In this series of computations, PE is characterized by varying the FCI electrical conductivity from 10^{-1} to 10^6 S/m for three different magnetic field strengths.

2. Problem specifications

A stainless steel rectangular duct containing an axial FCI is placed within a transverse fringing magnetic field. The FCI is placed within a segment of the duct equally offset from the inlet and outlet. The FCI features a PES of varying widths throughout the simulations. The configuration with a PES is illustrated in Fig. 1, and Fig. 4 demonstrates some slot width variations.

The cross-sectional dimensions of the duct and FCI are summarized in Table 1. Moving outward radially from the center of the duct is the bulk flow, the FCI, the gap, and the duct wall. In Table 2, the material electrical conductivities used in the computations are summarized.

Table 1
Cross-sectional dimensions.

Dimensions	Length [mm]	
Half-width of FCI box, b	23	
Half-height of FCI box, a	27	
Thickness of FCI, t_{FCI}	2	
Thickness of gap, t_{GAP}	5	
Thickness of slot, t_{SLOT}	3	Default
Thickness of wall, t_{wall}	2	

Table 2
Material electrical conductivities.

Component	Material	Conductivity [S/m]
liquid metal	In–Ga–Sn	3.34E+6
Duct	Stainless steel	1.40E+6
FCI	SiC	0 to 1.00E+6

A liquid metal eutectic of indium–galium–tin (In–Ga–Sn) flows uniformly at 5 cm/s into the duct inlet. At the outlet, a Neumann boundary condition is applied.

A fringing magnetic field is applied transversely. It varies from 0 to 1.8 T and is contained entirely within the length of the FCI. The fringing magnetic field equation is as described in Ref. [3].

The following boundary conditions are applied:

$\mathbf{n}\cdot\mathbf{j}=0$ at all outer surfaces, $U=5$ cm/s and $\partial p/\partial x$ at the inlet, and $\partial u/\partial x=0$ and $p=0$ at the outlet where $\mathbf{n}$ is the vector normal, $\mathbf{j}$ is the current density, and p is the pressure. A no-slip condition is also applied to fluid-solid interfaces while a symmetry boundary is applied at the $x-z$ mid-plane.

A 5.2 million element, rectangular, and collocated grid was constructed using HIMAG's built-in grid generator with 508, 92, and 56 cells in the x (axial), y, and z directions for the default case. The grid was partitioned, and the simulation was run in parallel on up to 256 cores. Mesh refinement simulations were performed to ensure accuracy consistency for macro-level results.

3. Results and discussion

To clearly describe the differences between the various measured flow characteristics herein, several parameters will be introduced. The total pressure drop, from the inlet to the outlet, will be notated as ΔP. The bulk pressure within the FCI and pressure in the gap (shown, along with others, in Fig. 5) will be notated with P_{BULK} and P_{GAP}, respectively. The pressure difference, or transverse pressure, between the bulk and gap flows, normalized by the gap pressure, will be notated as $\Delta_T P$.

To compare the two pressure equalization mechanisms in this study, the difference between the transverse pressure gradients with respect to the axial direction x in the bulk and gap flows will be inspected and calculated as in Eq. (5):

$$\Delta_T P' = \frac{d}{dx}\left[\frac{P_{BULK}-P_{GAP}}{P_{GAP}}\right] \quad (5)$$

where will we refer to as $\Delta_T P'$ as the "pressure difference parameter". P_{BULK} and P_{GAP} are not always uniformly distributed as analyzed in [8]. That is why in this study P_{BULK} is measured at the center of the duct, and P_{GAP} is measured in the center of the bottom gap (Fig. 5). $\Delta_T P'$ is measured over 500 mm centered in the axial direction, magnetic field, and the FCI. These gradients were relatively constant for a substantial section around the center of the FCI, where $x=0$. The transverse pressure gradient is presented normalized by the pressure gradient in the gap flow. *Note that a value of zero means that pressure is equalized in a cross-section and is desirable.*

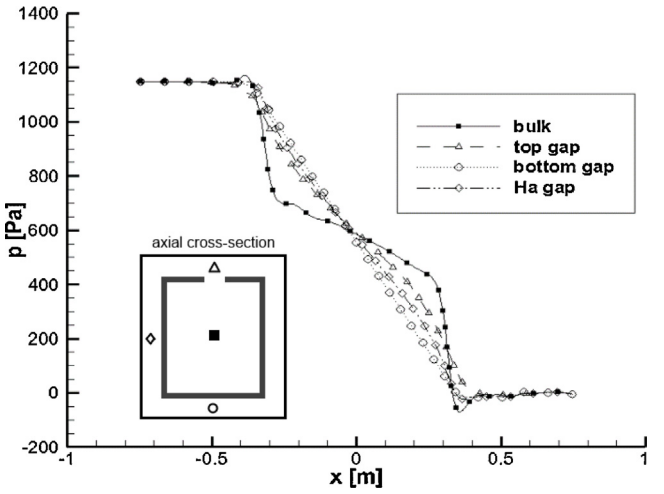

Fig. 5. This axial pressure vs. duct length plot illustrates the pressure difference between the bulk and gap flows. This figure includes the pressure equalization slot and $\sigma=0.1$ S/m.

3.1. Electromagnetic pressure equalization

Results from our investigation into the pressure equalization through Lorentz forces via electrical currents passing through the FCI are shown in Fig. 6. Considering the entire range of FCI conductivities from 0 S/m to values comparable to the LM, the transverse pressure difference becomes closer to equalized with increasing conductivity, which we have also directly shown in Fig. 8.

We conclude, expectedly, that this mechanism is successful in equalizing the pressure between the bulk and gap flows. In practice, however, the FCI insulating requirements and physical properties of SiC limit the range of allowable electrical conductivities to $\sim 10^2$ S/m.

Because the curves are approximately aligned, it appears that the FCI's effectiveness in pressure equalization as a function of electrical conductivity is relatively independent of the Hartmann number, or B-field strength. This finding may be applicable in an extrapolation to reactor-like conditions.

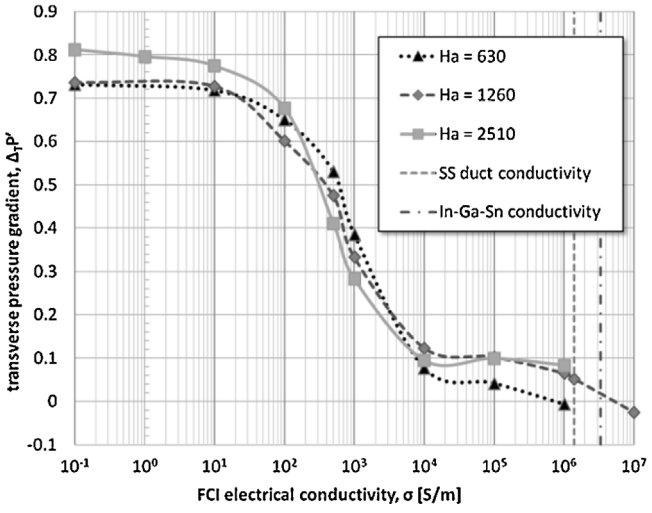

Fig. 6. The curves represent simulations over three *Ha* numbers corresponding to B0 values of 0.5, 1, and 2 T with no slot present. It appears that the transverse pressure gradient is relatively independent of the *Ha* number.

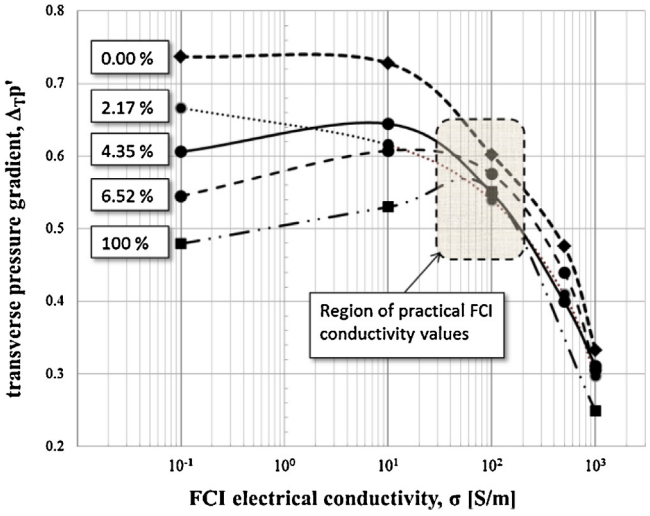

Fig. 7. The curves represent different PES widths as a percentage of the total sidewall width and show a trend toward convergence with increasing FCI conductivity regardless of the slot width.

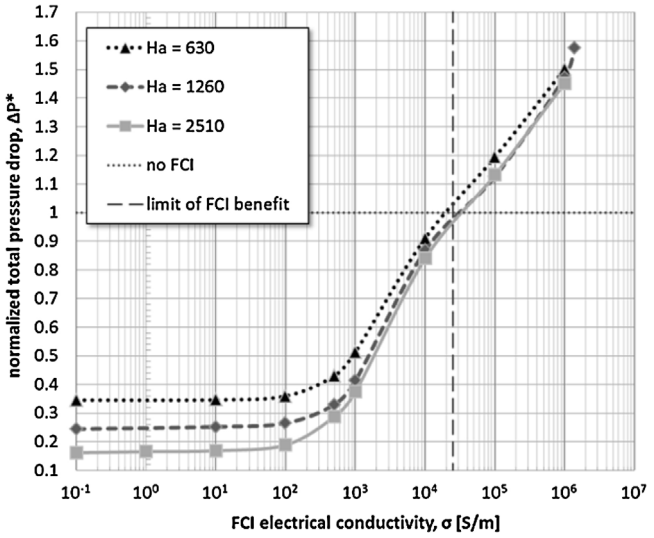

Fig. 9. Each curve (representing no slot cases) has been normalized by the pressure drop for a similar case with no FCI, and we reveal that the FCI is more effective for higher *Ha* numbers.

The curve in Fig. 6 with $Ha = 2510$ has the least PE for low and high electrical conductivity but, interestingly, has the best PE in the mid-range values, relative to other curves.

3.2. Hydrodynamic pressure equalization

Results where the PES width was modified over various FCI conductivities are shown in Fig. 7. At $\sigma = 10^{-1}$, the results follow intuition: the highest pressure difference parameter is that with no slot and the lowest occurs where the slot width comprises the entire sidewall (full-wall slot). Accordingly, the curves in Fig. 7 are labeled as a percentage of the slot width relative to the wall width. The advantage of hydrodynamic coupling with a slot remains as the FCI conductivity is increased but the range of $\Delta_T P'$ between having no slot and a full-wall slot drops dramatically.

Because a full-wall slot case with an ideally insulating FCI still has a normalized pressure difference parameter of approximately 0.48, we conclude that coupling the bulk and gap flows hydrodynamically with a slot in our configuration is not as an effective PE mechanism. Furthermore, as the FCI conductivity is increased, the presence of the slot appears to become insignificant (Fig. 7). At conductivities near 10^2 S/m, the range is reduced to ~0.1, whereas it was at ~0.25 for 10^{-1} S/m. It seems that continuing simulations into higher FCI conductivities will show that the curves for various slot widths will converge.

It is unclear why there is a trend of the pressure difference parameter increasing for a short range of FCI conductivities between 10^{-1} and 10^2 for the curves of the three widest openings.

3.3. Total pressure drop

The total pressure drop for each case is normalized by the pressure drop for a case with the same parameters but no FCI. We define this normalized total pressure drop as:

$$\Delta P^* = \frac{\Delta P}{\Delta P_{\text{no FCI}}} \tag{6}$$

Fig. 9 shows that the FCI insulating effect depends on the *Ha* number. In a stronger magnetic field, the effect is more pronounced. Beyond $\sigma = 10^3$ S/m, the curves approximately converge, revealing that the effectiveness becomes relatively independent of *Ha* number. FCI conductivities this high, however, are impractical.

The horizontal line in Fig. 9 represents the pressure drop for a duct with no FCI and serves as a baseline case. The vertical line shows the approximate value of the FCI conductivity where it is no longer effective at reducing the pressure drop. This value is approximately 2.5×10^4 S/m, so it is outside the range of design considerations. However, it may be important if damage to an FCI in a reactor reduces its insulation abilities.

Finally, we invert the normalized pressure drop to represent the *effectiveness* of an FCI, which we call the R factor, at various conductivities over a range of interaction paramters (Fig. 10). The interaction parameter is defined by:

$$N = \frac{Ha^2}{Re} \tag{7}$$

N is a ratio of the electromagnetic forces to inertial forces.

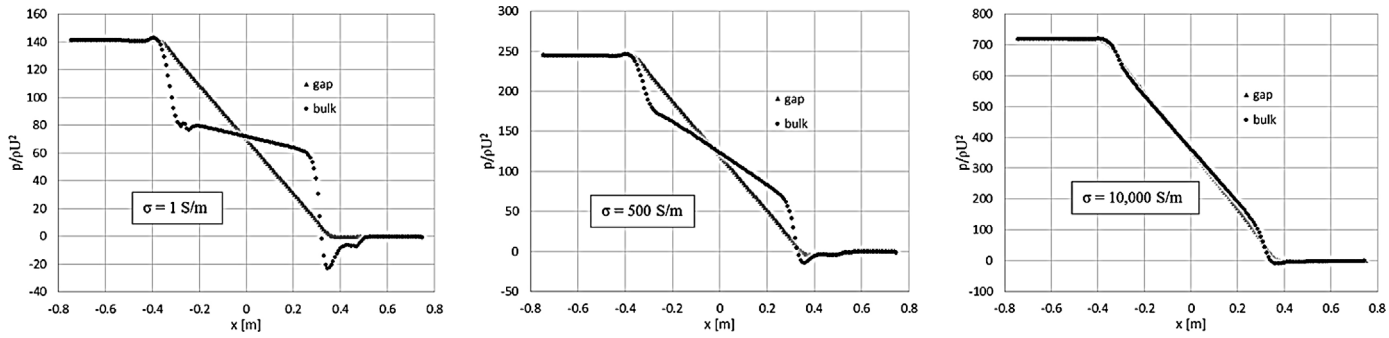

Fig. 8. Increasing the FCI electrical conductivity shows a clear trend toward pressure equalization.

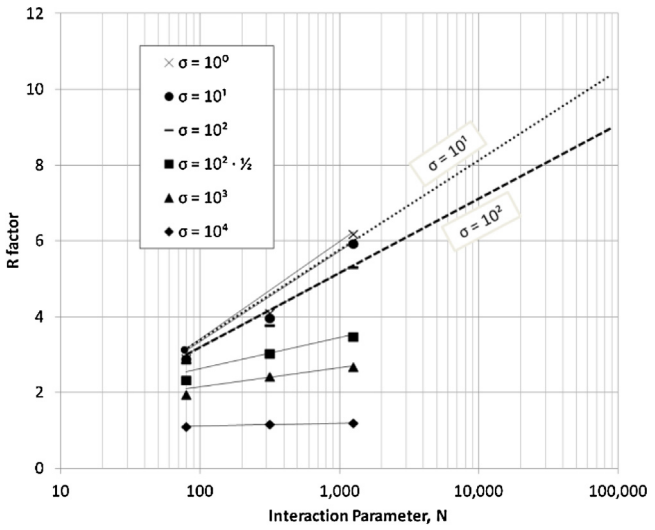

Fig. 10. Results are extrapolated to show that the FCI is more effective for higher interaction parameters.

The curve fits on this log plot are then extrapolated to interaction parameters at the orders of magnitude expected in ITER and future DEMO reactors. However, the isolated conditions of this simulation are not representative of practical configurations, and better R factors may be expected in these cases. We can see that the FCI is most effective at low conductivites and, desirably, increases as the interaction parameter increases.

4. Conclusions

Pressure in an axial cross-section of the duct can be equalized by Lorentz forces. However, considering practical values for the FCI conductivity, we conclude that the pressure will be only partially equalized. The effectiveness of pressure equalization via currents passing through the FCI appears to be independent of the *Ha* number.

Inclusion of a pressure equalization slot does help equalize the pressure in the axial cross-section of the duct, but even with a full-wall length slot, the equalization only reaches appromixately 50% according to our benchmark. Additionally, when practical conductivities for the FCI are considered, the differences in the effectiveness for no slot to full-wall length slots are within a 10% range. We also notice a perculiar trend of a decreasing pressure equalization effectiveness as the FCI conductivity increases (at a lower range of 10^{-1} to 10^{2} S/m) for some of the wider slots.

We conclude that a pressure equalization slot is not an effective choice for pressure equalization given pratical design considerations.

Acknowledgments

This work was performed with support from U.S. Department of Energy, Office of Fusion Energy Sciences, under Grant No. DE-FG02-86ER52123.

References

[1] M.S. Tillack, S. Malang, High performance PbLi blanket, in: Proceedings of the 17th IEE/NPSS Symposium on Fusion Engineering, vol. 2, 1997, pp. 1000–1004.
[2] S. Smolentsev, N. Morley, M. Abdou, MHD and thermal issues of the SiCf/SiC flow channel insert, Fusion Science and Technology 50 (2006) 107–119.
[3] D. Sutevski, S. Smolentsev, N. Morley, M. Abdou, 3D numerical study of MHD flow in a rectangular duct with a flow channel insert, Fusion Science and Technology 60 (2) (2011) 513–517.
[4] S. Smolentsev, Z. Xu, C. Pan, M. Abdou, Numerical and experimental studies of MHD flow in a rectangular duct with a non-conducting flow insert, Magnetohydrodynamics 46 (1) (2010) 99–111.
[5] Z. Xu, C. Pan, X. Zhang, L. Zhao, J. Zhang, G. Yang, Primary experimental results of MHD flow in the duct with flow channel insert, Nuclear Fusion and Plasma Physics 29 (2009) 6–9 (in Chinese).
[6] N.B. Morley, M.J. Ni, R. Munipalli, P.A. Huang, M.A. Abdou, MHD simulations of liquid metal flow through a toroidally oriented manifold, Fusion Engineeringand Design 83 (2008) 1335–1339.
[7] S. Smolentsev, N.B. Morley, C. Wong, M. Abdou, MHD and heat transfer considerations for the US DCLL blanket for DEMO and ITER TBM, Fusion Engineering and Design 83 (2008) 1788–1791.
[8] M.J. Ni, S.J. Xu, Z.H. Wang, N.M. Zhang, Simulation of MHD flows in liquid metal blanket with flow channel insert, Fusion Science and Technology 60 (2011) 292–297.